Carbonation rate and microstructural alterations of class G cement under geological storage conditions

Konstantinos Giannoukos[a,b*] Sean P. Rigby[b] Christopher A. Rochelle[c]

Antoni E. Milodowski[c] Matthew R. Hall [a,b]

a Nottingham Centre for Geomechanics, Faculty of Engineering, University of Nottingham, University Park, Nottingham NG7 2RD, UK

b Geo-Energy Research Centre**, Department of Chemical and Environmental Engineering, University of Nottingham, University Park, Nottingham NG7 2RD, UK

c British Geological Survey, Environmental Science Centre, Nicker Hill, Keyworth, Nottingham NG12 5GG, UK

The authors wish to acknowledge that this work was funded by the Geo-Energy Research Centre (GERC) and the Natural Environment Research Council (NERC). They kindly express their gratitude for the technical assistance of Nigel Neate and Martin Roe for their remarks on the SEM and the experimental assistance of Gemma Purser, Lauren Selby and Keith Bateman in the BGS Hydrothermal Laboratory. Christopher A. Rochelle publishes with the permission of the Executive Director of the British Geological Survey, UKRI.

Supporting Information

Details of the cement samples preparation, carbonation reactors and parameters of the SEM analysis are given at the supporting information. Images of the XRD data for the samples treated with the CO_2-saturated brine and N_2-saturated brine and other images from SEM analysis are also given at the supporting information.

*Now at: Elettra-Sincrotrone Trieste S.C.p.A., 34149 Basovizza, Trieste ITALY; e-mail address: kostas18ns@yahoo.com

**GERC was previously the Nottingham Centre for Carbon Capture and Storage (NCCCS)

Abstract

Cementitious grouts are a vital component for the economically-viable implementation of the geological storage of CO_2 in providing an engineered long-term seal. In this study a class G cement was carbonated at 80 bar, at either 60 ºC or 120 ºC, whilst immersed in a synthetic brine for durations of up to 5 months. X-ray computed tomography was used to evaluate the advancement of carbonation depth, whilst SEM/ EDXA and XRD were used to characterise microstructural alteration of the cement phases. The microstructure of the 'main carbonation front' was found to be representative of the governing reactive transport mechanism. An ill-defined 'main carbonation front' during carbonation at 80 bar /60ºC showed a carbonation mechanism controlled by the rate or precipitation/ dissolution reactions; diffusion in that case was not the controlling factor. The faster local supersaturation conditions in the pores at 60 ºC (with respect to Ca^{2+} and HCO_3^-) created a dynamic system of aragonite precipitation from the carbonated to the inner regions of the cement. At 80 bar/120 °C a clearly defined 'main carbonation front' with higher compositional density than at 60ºC, was correlated with the fast reactions and diffusion limited evolution of the 'main carbonation front'. Calcite, as the main result of those fast reactions at 120 ºC, filled ubiquitously previously unmineralized voids, creating a system less prone to compositional alterations by chemical changes due to the CO_2 plume. This study showed, that the formation of calcium carbonate polymorphs depends on the kinetics of carbonation reactions for a class G cement that is determined by temperature and time. The findings of the current paper can be further used for the the understanding of reaction processes within the cements of the CO_2 injection wells and assess their long-term chemical stability.

Keywords: geological storage, cement carbonation, rate of carbonation, carbonation front, reactive transport, calcium silicate hydrates, portlandite

1. Introduction

Securing investment in the geological storage of CO_2, together with addressing regulatory and public acceptance criteria, will require the demonstration of its long-term containment deep underground, negligible leakage of CO_2 from the injection wells, and an economic method of long-term monitoring of the wells. CO_2 from major emitters (mCO_2 >0.1Mt/yr[1]) has long been pumped into rocks deep underground, either onshore such as at the Weyburn field in Canada (since 2000 more than 20 Mt CO_2 injected at 1300-1500m depth) [2][3][4][5] or off-shore into deep saline aquifers below the sea floor such as at the Sleipner field in the North Sea (more than 10Mt CO_2 injected; 1Mt CO_2/year at 800-1000m) [6]. The primary CO_2 leakage risk can be attributed to the number of deep boreholes in the area [7], which appears larger than compared to the leakage through the caprock [8]. Consequently, a continued study of the wells as routes for CO_2 leakage is indispensable for the consolidation of the CCGS technologies. The results from such studies will add to existing expertise, and inform countries that have already adopted specific regulations on CO_2 geological storage, or 'geosequestration', (such as Canada, USA, UK and Australia) [9]. According to those regulations for minimizing the leakage pathways of injected CO_2, the importance of cementitious grouts for sealing the rock-borehole interface CCWs (Carbon Capture and storage Wells) has been well defined.

When CO_2 is dissolved into water it forms carbonic acid, which makes aqueous solutions slightly acidic[10]. Advection and diffusion of this into the pore network of cement causes "neutralization" of its alkaline pore fluid [11]. It was found that the initial dissolution of portlandite (CH) and the further dissociation of calcium silicate hydrate (C-S-H) phases, enhance the buffering action of CH [12] with the end product being amorphous silica gel and polymorphs of calcium carbonate ($CaCO_3$) [10]. Newly formed $CaCO_3$ can be found either at the locations of CH and C-S-H dissolution or within the intact cement owing to the diffusive

transport of species through the pore network [13]. The accumulation of $CaCO_3$ may form a 'reaction front' that hinders further CO_2 diffusion, thereby protecting reactive components (CH and C-S-H) within the unreacted regions of cement [14]. Experimental evidence has demonstrated that the shape of the reaction fronts is highly influenced by the interactions of the cement paste along interfaces with the contacting rocks [15] and borehole steel [16]. The correlation of the evolution of the reaction front with the mineralogical alterations during carbonation has been studied using numerical [17] and experimental [18] models. Cement core samples from real CO_2 injection sites [19] [20] [21], have been compared with laboratory samples carbonated at various T,P conditions for either their mineralogy [22] or the rate of carbonation reactions [23]. Despite the understanding of the $CaCO_3$ formation in natural systems [24], the correlation of the $CaCO_3$ polymorph with the rate of carbonation and mineralogy remains poorly understood [25]. Little is known concerning the microstructure of the fronts in the particular case of cement carbonation and the correlation of the shape of the fronts with the governing transport mechanism. The quantification of the shape of the fronts in heterogeneous media has been proposed in the literature in terms of the spreading of the front [26]. The quantification of the front is not our goal in this paper, but rather a description in qualitative terms. The initial hypothesis is that diffusion-limited transport will create clearly visible fronts (high compositional density), while reaction-limited transport will lead to ill-defined fronts. The latter means fronts, with compositional density similar to the reacted and unreacted regions, with large spreading values according to [26].

Assuming proper cementing practices [27] a cementitious grout needs to tolerate carbonation rates that would allow the assimilation of the injected and dissolved CO_2 from the reservoirs rock formations [28]. Cementing practices providing a well hardened and secure cementitious grout for securing zonal isolation with no cracks should be verified from the well contractors [29]. The injected cement forms a critical seal and needs to be engineered such that

its carbonated regions would not allow fast chemical degradation of the cement phases [30] leading to fluid flow. Many studies have focused on the mineral alterations of cements using electron microscopy and X-ray diffraction before and after carbonation [31][32]. Other studies have used X-ray tomography to measure the kinetics of carbonation reactions and to predict the times for full degradation of a cement sheath [33]. Despite detailed knowledge about the formation of calcium carbonates and conditions needed to favour a specific polymorph [34], no study, to the best of the knowledge of the authors, has correlated carbonate phases (e.g. calcite, aragonite, vaterite) with the rate of carbonation under realistic downhole conditions. The purpose of the correlation of the downhole conditions with the type(s) of carbonate polymorph that form(s), could allow for faster characterization of cement for its carbonation resistance (via core drilling or cement bond logs), during the monitoring stages of injection and abandonment. Despite there being studies of $CaCO_3$ polymorphs under various conditions during CO_2 mineralization [35], little is known about the characteristic polymorph(s) formed during cement carbonation. In other words, this study will link: the carbonation kinetics at various temperatures; the preferential calcium carbonate polymorph; and phase alterations of the cement hydrates. Though studies exist on these topics, their scope is limited to one or two topics each time. Our results are expected to provide a practical understanding for academia and industry concerning monitoring studies of cement carbonation and long-term stability in real injection wells, respectively.

In this study we aimed to determine the:

- Microstructural alteration of a class G oilwell cement grout before, and after, accelerated carbonation in a synthetic brine
- Effect of temperature and pressure conditions on the reactive transport process during carbonation by evaluating the spatial distribution of reaction products within the cement microstructure

2. Materials and methods

Cement-based pastes were produced in line with standard mixing protocols [14] for grouts used to seal the annular gap between the steel borehole liner and the surrounding rock formations of the Sleipner field operating in the North Sea. Mixing was done using a Hobart A120 – 12-Quart All Purpose Mixer and the samples were generated using cylindrical molds with a diameter of 4.7cm and height of 2cm. The curing procedure is explained in the Supporting Information.

The experiments were conducted at a constant pressure of 80bar (8MPa) in batch reactors operating at 60ºC for 1 and 5 months, or at 120ºC for 1 and 3 months. Further details of the reactors are given in a previous study [14] and in the Supporting Information. In order to aid sample tracking, at the end of each experiment, every sample was assigned a specific code unique to each sample. The first part of this code indicated the type of gas used to pressurise the experiment ('N' for N_2, and 'CO' for CO_2), the second part indicated the temperature of the experiment ('60' for 60ºC, and '120' for 120ºC), and the third part denoted the duration in months. For example, the 'N60/1' was used for the sample immersed in N_2-saturated brine at 60ºC for 1 month, and the "CO120/3" was used for the sample immersed in CO_2 saturated brine at 120ºC for 3 months.

The techniques used were what we had available to us at the time, and thought that SEM with XRD would suffice for this study. Backscattered electron (BSE) imaging was undertaken on polished and conductive surfaces using an XL30 SEM made by Philips, and equipped with an energy dispersive analysis X-ray (EDXA) detector offering the opportunity for simultaneous phase differentiation and elemental mapping. Details of the sample preparation and instrument parameters are given in the Supporting Information. Details of the

150 elemental mapping by EDXA are also given in the Supporting Information. XRD powder
151 analysis was conducted using a Siemens D500 diffractometer in Bragg-Brantano geometry
152 using a Cu Kα irradiation source with wavelength 1.5406 Å. Analysis was conducted for 2θ
153 angles across the range 5º to 80º at a scanning rate of 0.05º and a step time of 4 seconds. A
154 powder using an agate mortar and pestle was produced for the XRD analysis and was placed
155 carefully into the sample holder, so as a perfectly flat surface to be created. The limited quantity
156 of the powders for the carbonated parts did not allow for a sophisticated method for production
157 of powders with mean particle diameter less than 2 μm [36]. The employed method of hand
158 mortar and pestle was deemed to be successful for 'standard resolution'-type XRD powder
159 characterisation studies [37]. In order to obtain non-destructive 3D volume imaging of the
160 whole reacted and unreacted samples, X-Ray computed tomography (XRCT) was performed
161 using an XRADIA VERSA XRM-500. The image size was 2048 pixels*2048 pixels, the pixel
162 size was 25μm, the exposure time was 5 seconds, the camera readout setting was set to fast
163 (2.5MHz), and the source voltage was 160kV. For the post-processing and visualisation of the
164 alteration due carbonation, Dragonfly 2020.1.1.809 was used under academic license
165 (Dragonfly 3.7.3 [Windows]. Object Research Systems (ORS) Inc, Montreal, Canada, 2018;
166 software available at http://www.theobjects.com/dragonfly).

167

168 **3. Results and Discussion**

169 BSE micrographs of samples reacted with the carbonated brine showed two distinct
170 regions that were separated by a visually apparent 'main carbonation front' (see Figure 1).
171 Analysis of the Ca/Si ratio graphs has shown, not a rapid leaching of Ca to the brine, but a
172 controlled transport, reaction and precipitation of Ca and carbonates throughout the cement
173 matrix. Figure 2 shows the Ca/Si profile from the surface to the inner region of cement
174 calculated from the Ca and Si EDXA elemental maps. The inner region is defined here as the

175 ‘unreacted core’ of cement in advance of the ‘main carbonation front’ and with a microstructure
176 similar to the unreacted sample as observed from BSE micrographs. The term inner ‘core’ is
177 not used in our study, since it might induce confusion with the ‘cores’ of cement from sampling
178 in oilwells. Nevertheless, the inner region of cement (or simply inner region) is anticipated to
179 experience microstructural alterations due to chemical and thermal gradients. Big variations in
180 Ca/Si on the outer edge of the carbonated region are due to severe decalcification due to Ca
181 transport towards the surface and subsequent leaching to solution. Zones with steady Ca/Si
182 ratio (*e.g.* for samples CO60/1 and CO120/1, see Figure 2) from 0.25 mm to 0.50 mm, showed
183 that the decalcification of the C-S-H phases took place gradually despite the temperature
184 difference. In other words, decalcification was not a step function at the ‘main carbonation
185 front’, but a controlled process at 60℃ and 120℃. Possible limitations in the Ca transport were
186 not attributed to differences in chemistry, but were associated with the pathways for diffusion
187 (see Figure 2). Diffusion limited reactions seemed to be synchronized (spatially) in a
188 continuous main reaction front, which at 120℃ was observed to be characterised by greater
189 average atomic number deposition in terms of BSE imaging (than at 60℃) (see Figure 1). The
190 term ‘main reaction front’ or ‘main carbonation front’ refers just to the relatively narrow main
191 front of carbonation towards the centre of the sample over time that is clearly visible from the
192 BSE micrographs (see Figure 1) and separates a carbonated region from an inner cement
193 region. The ‘main carbonation front’ at 120℃ was observed as a single front (no relic fronts at
194 the carbonated region), while at 60℃ it was the newest front (from a series of minor ones within
195 the carbonated region) located in between the inner and carbonated regions (see Figure 2). At
196 60℃ the ‘main carbonation front’ was, rather, the precipitation front, of ongoing dissolution/
197 precipitation fronts (from the surface of the sample towards its centre), which upon dissolution
198 would lead to carbonation of non-carbonated cement phases. Those ‘minor’ (relic) fronts were

characterized with similar composition to each other, as far as the average Ca/Si ratio is concerned (see Figure 2).

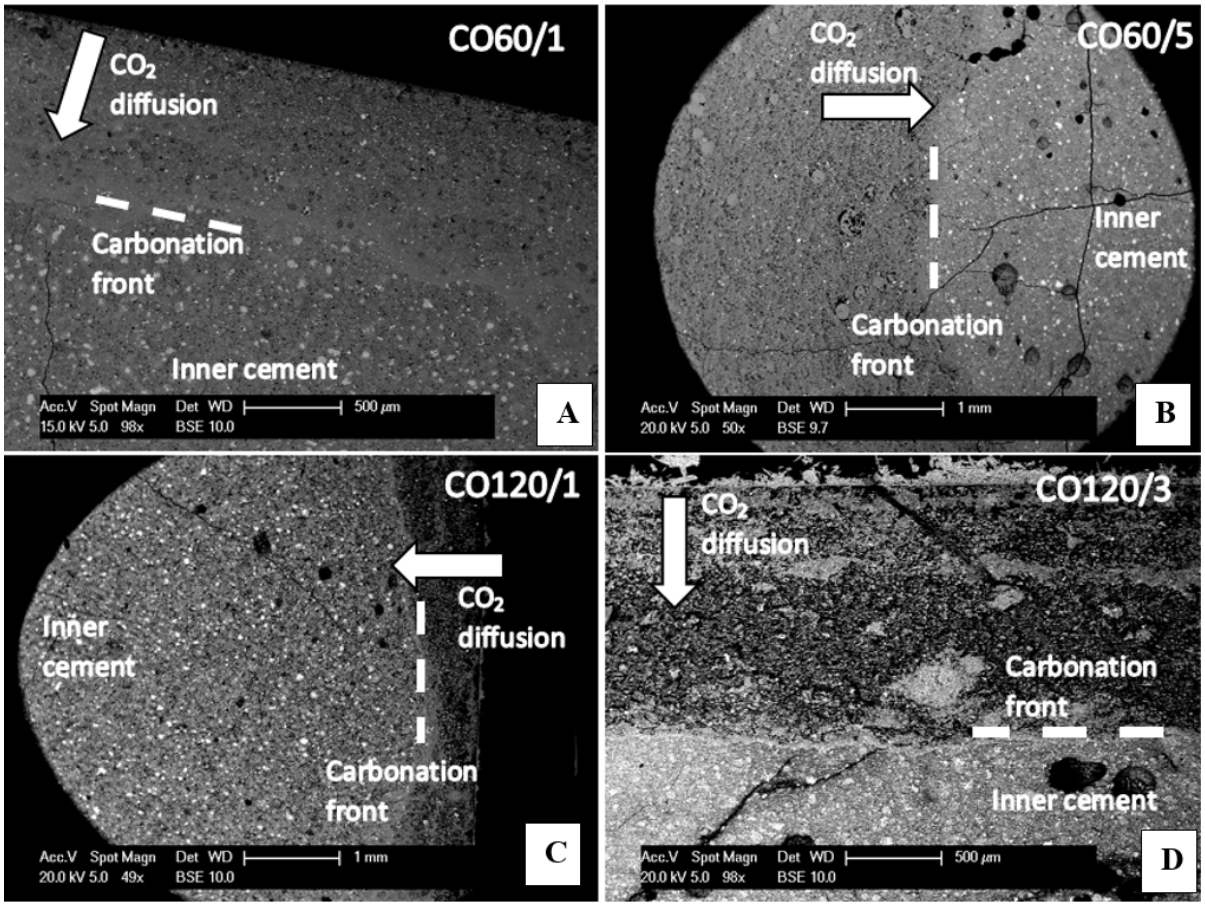

Figure 1 Backscattered electron micrographs for the samples immersed into carbonated brine at: (A)60ºC, 1 month; (B) 60ºC, 5 months; (C) 120ºC, 1 month; (D) 120ºC, 3 months. The CO_2 diffusion is simplified at the diffusion of the slightly acidic carbonated fluid of our study that contains $CO_2(aq)$ (HCO_3^-) and other studies with true carbonic acid.

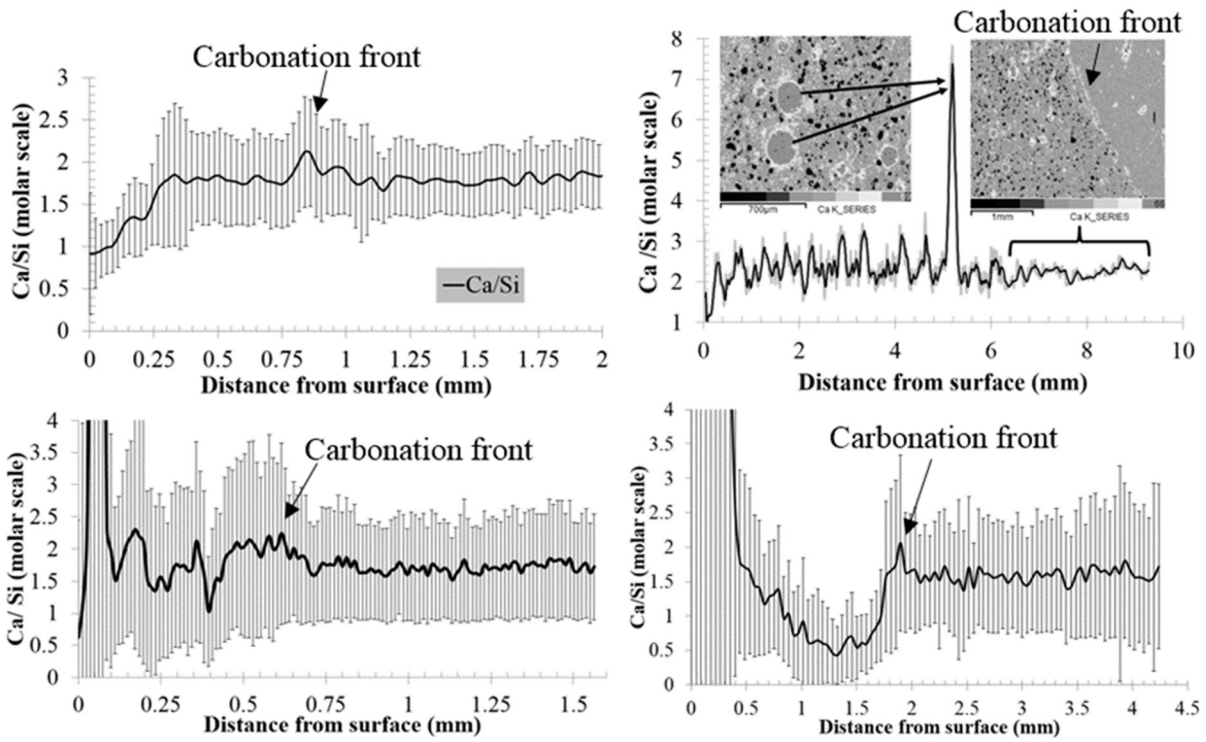

205

206 *Figure 2 Spatial profile of the Ca/Si ratio for the samples immersed in the carbonated brine at 60ºC and 120º; the calculation*
207 *steps of the Ca/Si ratio for each sample are shown in the Supporting Information.*

208 The outer zones of the samples, from the surface to the 'main carbonation front', were
209 characterized by major calcium carbonate precipitation. The 'main carbonation front' was the
210 latest of all the calcium carbonate precipitation fronts to form. That said, precipitation of
211 calcium carbonates depended on temperature. XRD analyses showed that calcite and aragonite
212 were produced at both temperatures and durations tested, and that vaterite was absent only
213 following treatment at 120ºC after 3 months reaction (CO120/3), according to XRD analyses
214 (see Figure 3) and SE imaging (see Figure 5). The diffraction peaks for the different
215 polymorphs of calcium carbonate in Figure 3 shows clearly the loss of vaterite in sample
216 CO120/3 at 2θ=25°, while the main peaks of calcite (2θ=30°) and aragonite (2θ=26°, 27° and
217 34°) are preserved. Amorphous $CaCO_3$ might be anticipated to form, before transforming to
218 one of the more stable polymorphs *i.e.* vaterite, aragonite and calcite. However, this cannot be
219 detected by XRD analysis.

The carbonate precipitation was found to be a dynamic phenomenon that reflected local saturation conditions with respect to ions of calcium and carbonates/bicarbonates. The morphological characteristics of the calcium carbonate observed by secondary electron (SE) imaging are consistent with the existence of the carbonate polymorphs identified using XRD. SE image analysis revealed evidence of the formation of new, stable and corroded aragonite crystals (depending on location in the sample) at 60ºC showing a dynamic system of carbonation reactions involving both precipitation and dissolution (see Figure 6 and Figure 8). Voids filled with rhombohedral calcite at 120ºC were evident as shown in Figure 5A, while aragonite crystals were also evident at 120ºC from crushed samples of the carbonated region of CO120/3 (see Figure 5B). Orthorhombic crystals of aragonite were also identified at 60ºC as shown for sample CO60/5 (see Figure 7). These represent air bubbles included in the cement paste during the cement manufacture/pouring process, and 'air voids' is a shorthand term being used here. These provide small micro-environments in which crystals can grow and which can be studied via the SEM. This suggests that extensive precipitation of multiple forms of aragonite from the carbonated zone (dense crystals) to the 'main carbonation front' (random small needles) may have occurred. The carbonate precipitation for sample CO60/5 was found to occur even to the inner region of the sample, in close proximity to the 'main carbonation front', with well-defined stable crystals of aragonite (see Figure 3 and Figure 8). Vaterite and calcite were not observed macroscopically in the CO60/5 sample, with SEM imaging only revealing small crystals among the decalcified C-S-H phases. Hence, at 60ºC, it appeared that the preferential formation of calcite and vaterite replacing the C-S-H matrix phases, and the aragonite precipitation in larger open porosity, were controlled by specific mass transport mechanisms. Those mechanisms allowed for controlled formation of calcite and vaterite in micropores, and aragonite to be ubiquitous in former air voids.

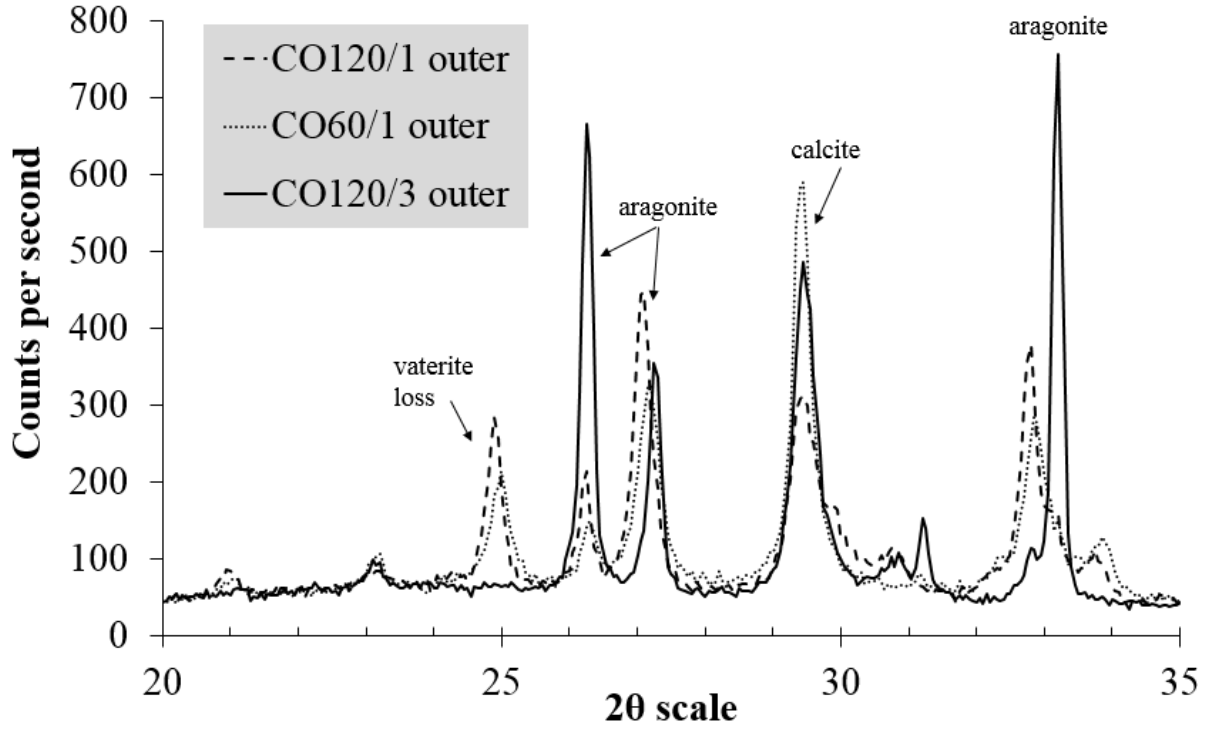

244

245 *Figure 3 XRD diffractograms of the samples immersed in CO_2 saturated brine at 60°C and 120°C.*

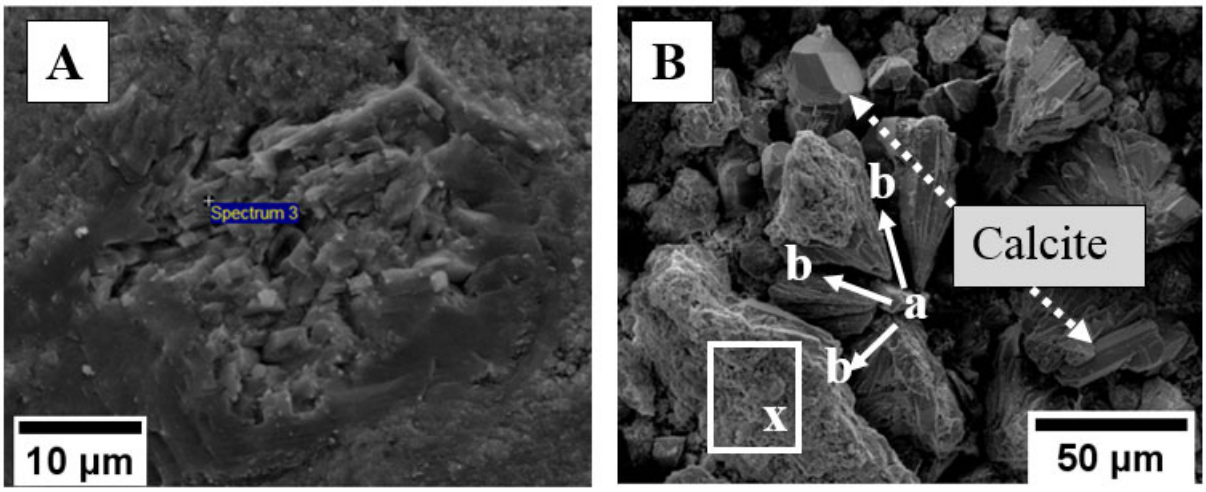

246

247 *Figure 4 Calcium carbonates at the carbonated parts of the CO120/ 1; (A) Blocky calcite crystals (with rhombohedral*
248 *cleavage) growth inside an air void; (B) aragonite crystals of a crushed sample; the area "x" shows vaterite with a*
249 *"cauliflower" morphology as a precursor for the aragonite growth in the direction of the arrows a→ b*

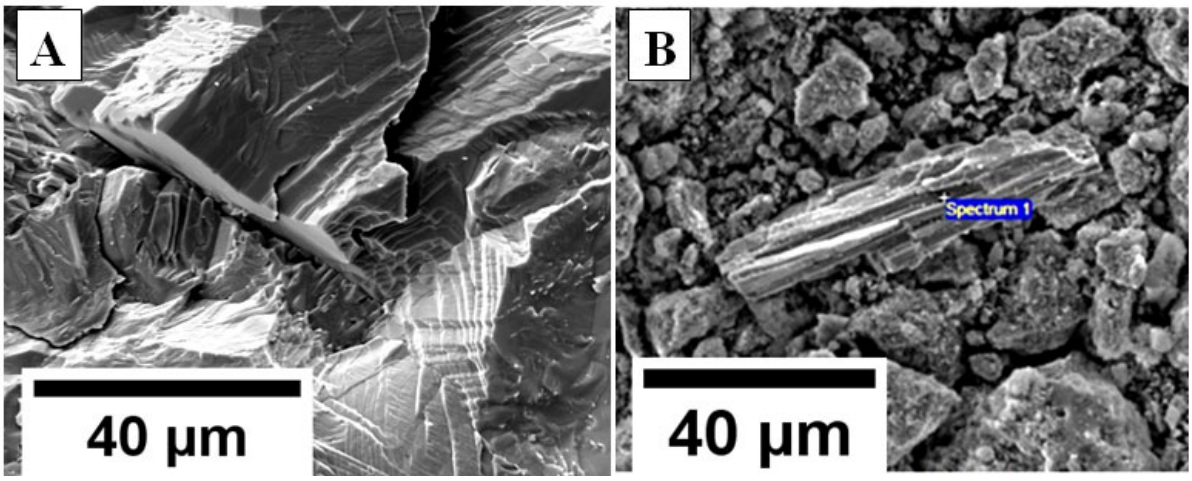

Figure 5 Calcium carbonates at the carbonated parts of the CO120/ 3; (A) Calcite crystals (with characteristic rhombohedral morphology) growth inside an air void; (B) aragonite crystals (with characteristic acicular-prismatic morphology) of a crushed sample; no morphologically-different vaterite was detected for any crushed samples.

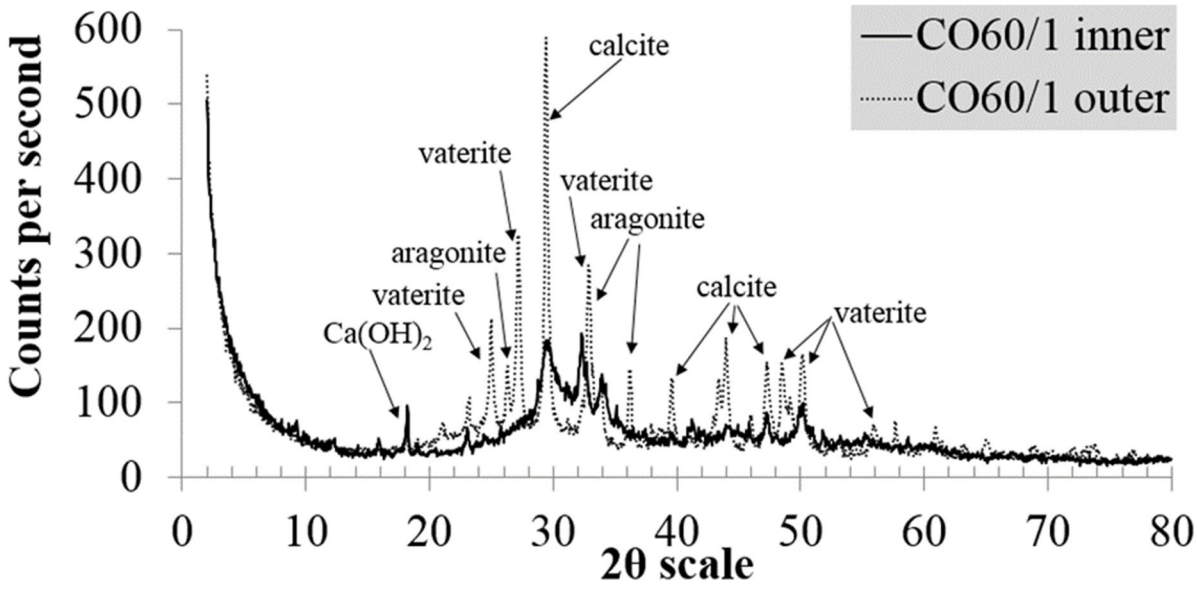

Figure 6 XRD diffractogram for the inner and outer regions of sample treated with carbonated brine at 60°C after 1 month

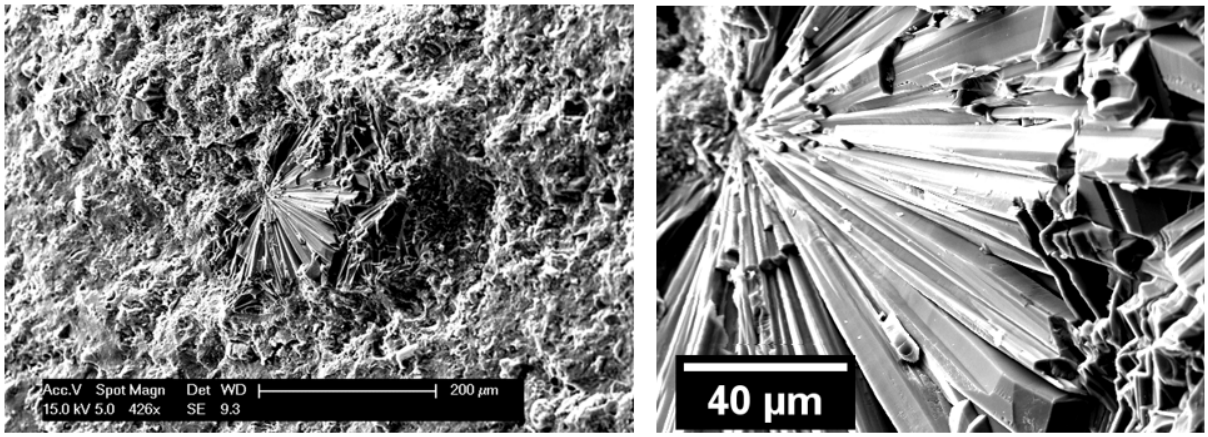

Figure 7 Wide field and close-up images of aragonite crystals growth inside an air void at a distance 3mm from the outer surface of the carbonated region of CO60/ 5

At 120ºC, the dynamics of the carbonation reactions were found to be reflected in the formation of stable calcite crystals that appeared to completely fill pre-existing voids (see Figure 4 and Figure 5). The carbonated regions at 120ºC showed a less transitional system, compared to that at 60ºC, with calcite formed rapidly rather than the metastable aragonite formed at 60ºC. At 120ºC, calcite, aragonite and vaterite (same range of polymorphism as in CO60) were found exclusively in the carbonated regions of CO120/1 and CO120/3 (see Figure 3). Calcite appeared to be the major calcium carbonate, filling the air voids almost ubiquitously, and was evident macroscopically in SEM images irrespective of time. Vaterite was not detected microscopically during SEM examination of entire cement blocks but only as calcium carbonate with "cauliflower-morphology" in crushed samples (see Figure 4). In fractured blocks of the carbonated regions at 120ºC after 1 month, vaterite was found as part of the same structure as aragonite crystals showing a dynamic system of continuously transforming calcium carbonates via phase precipitation changes over time (sample CO120/1) (see Figure 4). Those changes could have happened via actual solid-state phase transformations, possibly as a mechanism of fast dissolution of the unstable polymorph and fast re-precipitation of the most favorable polymorph. This system provided evidence that the degree of supersaturation is changing, with vaterite forming rapidly at high degrees of $CaCO_3$ supersaturation, and

277 aragonite forming at lower ones. Although calcite may expected to be the most
278 thermodynamically stable phase, the precipitation of the calcium carbonate polymorphs may
279 be kinetically-controlled, with vaterite being the fastest, then aragonite, and then calcite.
280 Vaterite appeared initially quickly with dissolution of cement phases, giving relatively high
281 concentrations in solutions that favoured vaterite precipitation (sample CO120/1). For sample
282 CO120/3 the loss of vaterite (see Figure 3) was followed by a slowing down of dissolution
283 leading to lower concentrations/degrees of saturation, which favoured aragonite and calcite
284 (see Figure 5).

285 Cement samples immersed in N_2-saturated brine (*i.e.* a CO_2-free system, effectively an
286 experimental blank) provided evidence for the source of Ca (from the cement phases) that was
287 consumed during the carbonation reactions. For the samples subjected to carbonation, the
288 transport of Ca is complex, due to the Ca dissociated from the cement phases and the re-
289 dissolution of the calcium carbonates from the 'main carbonation front' towards the surface
290 and the centre of the sample. Comparisons of the non-carbonated to the carbonated samples,
291 has provided insights into the Ca transport from the cement phases, with no impact from the
292 carbonated brine. Thus, the usefulness of the non-carbonated samples was that they provided a
293 clear understanding of the Ca origin variation with temperature and the rate of mobility of the
294 Ca cations without the complicated transport due to carbonation reactions.

295 In samples subjected to carbonation, the mobility of Ca cannot be attributed solely to
296 the cement phases of the inner regions of the samples, but to the dissolution of old reaction
297 fronts, followed by Ca transport and re-precipitation at new carbonation fronts. As seen from
298 Figure 2, the carbonation depth is characterized by locations with a Ca/Si ratio equal or even
299 higher than that of the main front. Ca transport takes place from the cement phases of the inner
300 regions of the samples towards the main front along with the Ca dissociated from carbonated
301 areas and transported towards the main front. This transport requires directions of diffusion in

opposite directions, both with, and counter to, the direction of movement of the carbonation front. The driver for this is the increasing acidity: at higher pH to destabilise portlandite/CSH; and at lower pH to destabilise $CaCO_3$. The calculations of the Ca concentration of the cement samples were based on the elemental maps using EDXA. The presence or absence of portlandite in the XRD diffractograms was used as evidence of its contribution of Ca to the carbonation reactions. In other words, the XRD diffractograms showing portlandite present suggested that both portlandite and, progressively, C-S-H supplied the Ca towards the outer areas of the cement, and prevented portlandite depletion (being the phase most likely to dissolve first [38]).

The source of Ca for the carbonation reactions at 60ºC was identified as both portlandite and C-S-H since both were present after 1 month reaction, irrespective of the type of brine, be it N_2-saturated or carbonated (see Figure S3, Supporting Information). After 5 months, due to portlandite loss, just the C-S-H phases from the inner region of CO60/5 were able to supply the Ca for the neutralization of the ingressing acidity and inorganic carbon species (see Figure S2, Supporting Information). It is evident (using the methodology of [39]) that the source of Ca was CSH phases from the centre of the sample, which when dissociated caused the Ca/ Si ratio to decline from 1.60 (for the unreacted sample grout) to 1.34 (for the N60/1), and then to 1.36 (for the N60/5). Carbonation reactions were found to proceed as a front, decalcifying all cement phases, such as C-S-H, Aft, AFm and C-A-H. However, the C-S-H of the inner regions of the sample also appeared to contribute Ca to the carbonation reactions by losing a part of the Ca and thus evolving to a lower Ca/Si ratio CSH. The front is more like a ‘zone’ which contains a visually obvious ‘main carbonation front’ where the microstructure is massively changed. But there are still changes going on either side of this front. To sum up, we find that, at 60ºC and 80bar, from XRD and EDXA analyses: (1) the chemical instability of portlandite during carbonation due to combined thermal and acidic conditions, and (2) the early/delayed

decalcification, per temperature and time, of the C-S-H phases as observed from the Ca/Si ratio of the inner C-S-H phases.

A comparison of observations of samples immersed in carbonated brine at 120°C, or in nitrogen-saturated brine, has provided evidence for the source of Ca. XRD analysis of sample N120/1 showed that the majority of Ca emanated from the complete dissociation of portlandite (see Figure S3, Supporting Information). Additional evidence of the dissociation of portlandite was found from the ICP-AES analysis of the post-reaction fluids for the N120 samples. The Ca concentration of the post-reaction brines was found to increase from 410 mg/l (initial brine) to 1061 mg/l (N120/1), while at 60ºC Ca, in the post-treatment brine, it was measured to only be 795 mg/l (N60/1). Here we need to take into account two points. On the one hand that the sample is actively carbonating, so only the very outside of the sample may be in equilibrium with the solution. The central parts of the sample may be very out of equilibrium with it – it is just that the acidic fluid surrounding the sample has not managed to get in and react yet. On the other hand, these fluids are in equilibrium with calcite – the stable phase for cement carbonation and what will control Ca in solution. The values should thus reflect calcite saturation at that specific P & T. The dissociation of portlandite for sample N120/1 allowed for the Ca/Si ratio of the inner C-S-H phases (colloidal model [40]) to remain constant at 1.60, as with the unreacted sample. Even though the quantity of portlandite was not measured, the experimental evidence suggests that, at the composition and curing conditions of the cement mix used, portlandite dissolved first as it was more reactive, and thus prevented the early dissolution of the C-S-H phases. CSH dissolution due to increasing temperature could have played a role in increasing the dissolved Ca, but was not a parameter in our study. After 3 months reaction, the inner C-S-H phases in the central parts of the sample appeared to decrease from Ca/ Si= 1.60 (unreacted sample) to Ca/ Si= 1.49. At 120ºC for the carbonated samples,

the early buffering of the carbonated brine appeared to be more effective than at 60ºC, with no evidence of carbonation at 120ºC beyond the carbonation front.

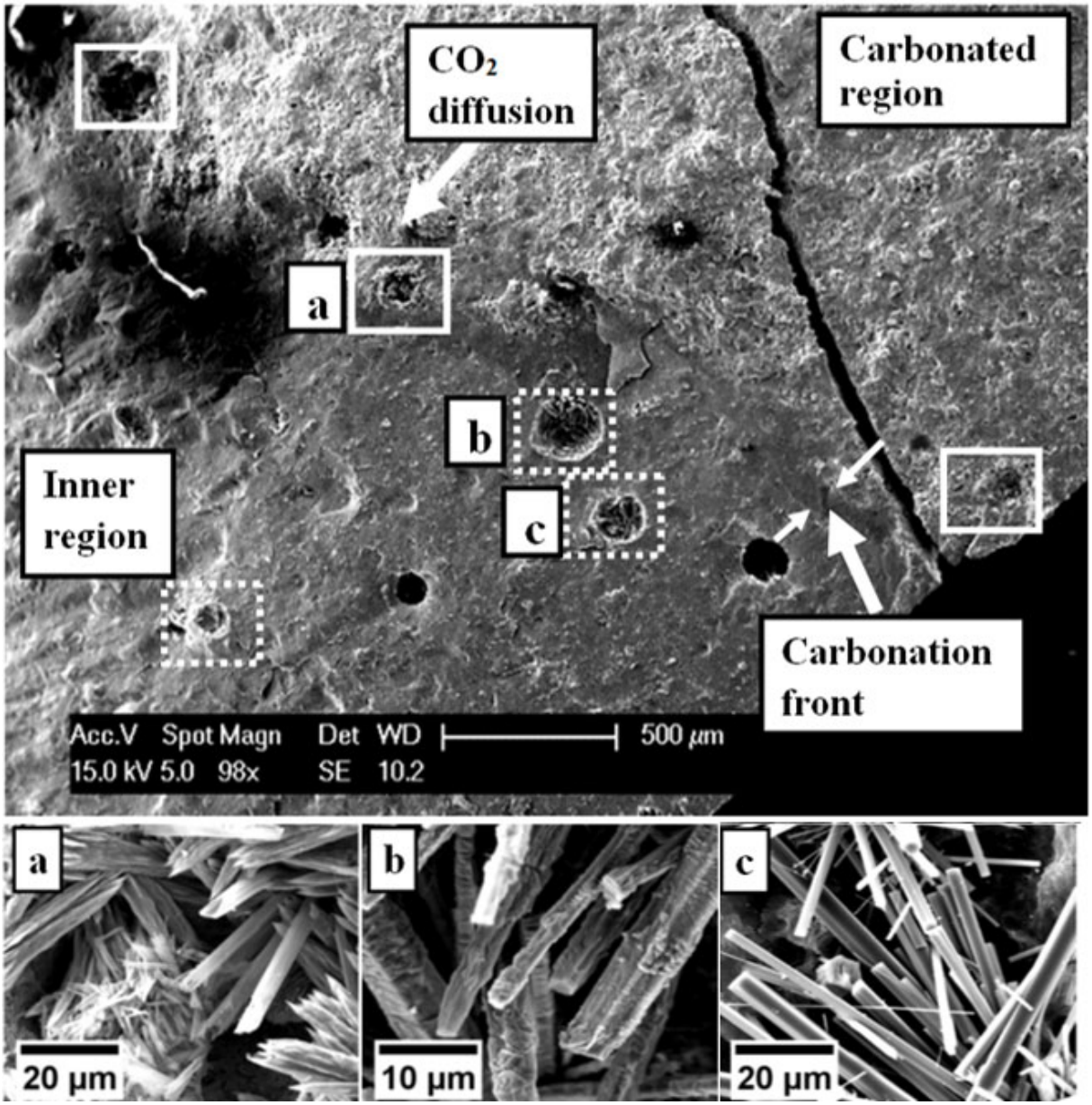

Figure 8 SE image showing the interface (carbonation front) separating the carbonated region and the inner region for the CO60/ 5. Air filled voids are also shown; frames with continuous lines, near carbonation front; frames with dotted lines, inner region. (a) Newly formed aragonite crystals growing inside air voids at the boundary of the carbonation front, (b) Aragonite crystals at a metastable state at the inner region and (c) Stable crystals of aragonite.

Figure 9 shows 3D tomographic reconstructions of samples treated with nitrogen-saturated brine and carbonated brine, which were generated using X-ray CT and Avizo Fire v8.1 image processing software. CT was only used to measure the depth of carbonation. The resolution of 25 μm was too low to allow for the reconstruction of a 3D connected network. Details of the carbonation depth of the samples immersed in the carbonated brine are shown in Figure 11. In addition, the segmented carbonation fronts are shown in Figure 12. It is notable the shape of the relic fronts at sample CO60/5, with the aragonite filled voids to be heterogeneously distributed amongst those fronts. Rigorous analysis of the pore connectivity (see Figure 12) was not an objective of the work reported here, and will be described in detail in a subsequent paper. Figure 10 illustrates an example of a sample immersed into carbonated brine and its evolution over time at 120℃ and at 60℃. The location of the measurement of the carbonation depth was chosen from the part of each sample facing upwards, in order to avoid areas close to the sides of the reactor, and that might possibly give smaller depths due to insufficient mixing of CO_2 with the brine.

In contrast to the local heterogeneities at the scale of a few μm found with electron microscopy, XRCT allowed the calculation of a consistent carbonation depth that parallels the outer surface of the sample. The calculated carbonation depths and corresponding rates are shown in Table 1. The calculations for 14 days were done for comparisons with similar studies on rate of carbonation front [33]. We find that the carbonation rate after 5 months at 60℃ is tenfold the rate at 120℃. The Elovich equation for activated chemical adsorption [10] , provided a statistically poor fit to the experimental data, but a power law fit the data better. We tentatively suggest that penetration depth and CO_2 sorption kinetics vary significantly according to the type(s) of polymorph formed. The migration of the reaction fronts appeared to have a rate of change that accorded with the square-root of elapsed time law at 120℃, but not at 60℃ (see Figure 10). In other words, the rates of carbonation reactions at 120℃ after 1

month (CO120/1) and after 3 months (CO120/3) appeared to be the same. In contrast, the rates of carbonation reactions at 60℃ after 1 month (CO60/1) and after 5 months (CO60/5) appeared to differ by an order of magnitude, despite similar rates being observed after 1 month at 120℃ (CO120/1) and 60℃ (CO60/1) (see Table 1).

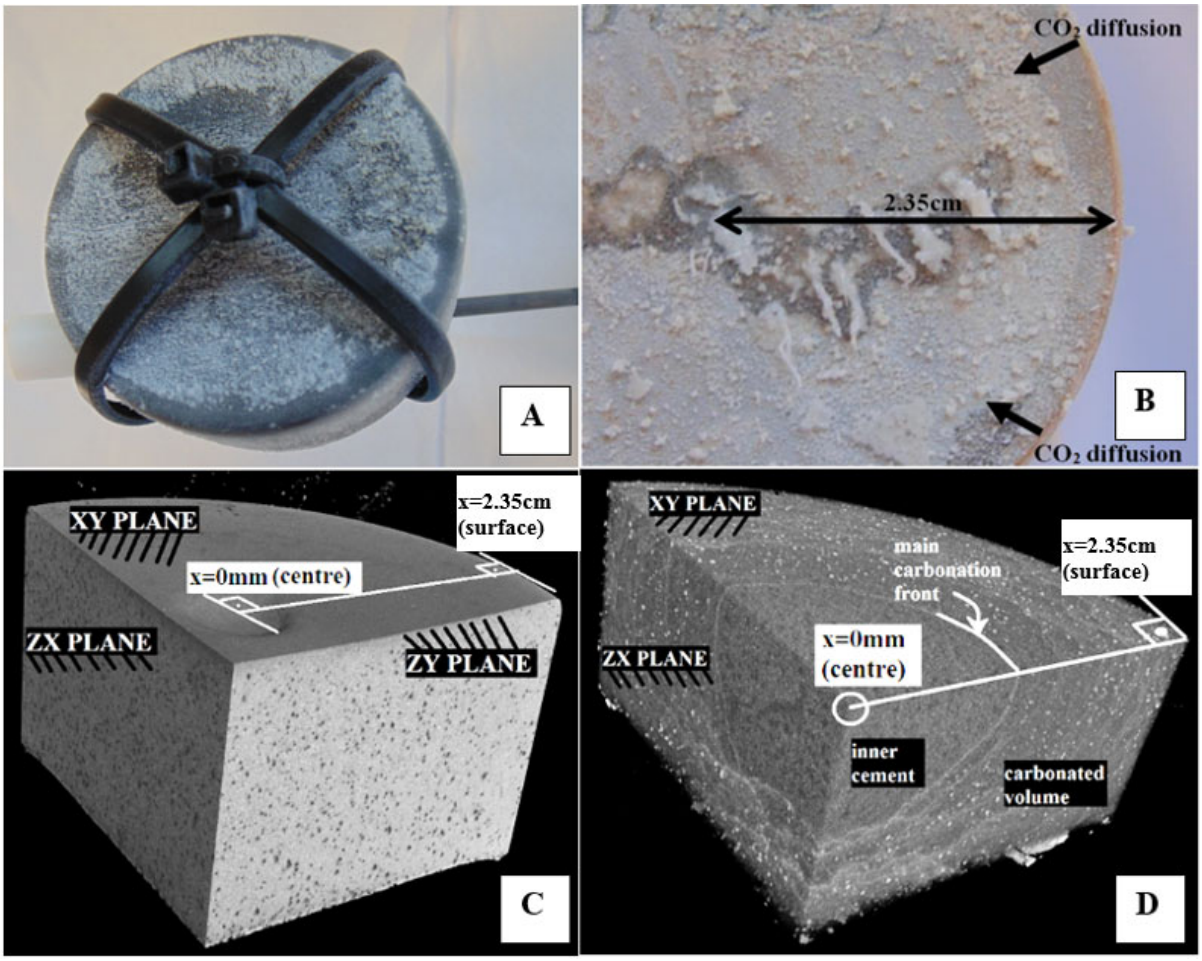

Figure 9(A) Sample N60/5 and (B) Sample CO120/3 after removal from the respective reactors; (C) X-ray tomographic volume section of the N60/ 5; (D) X-ray tomographic volume section of the CO60/ 5.

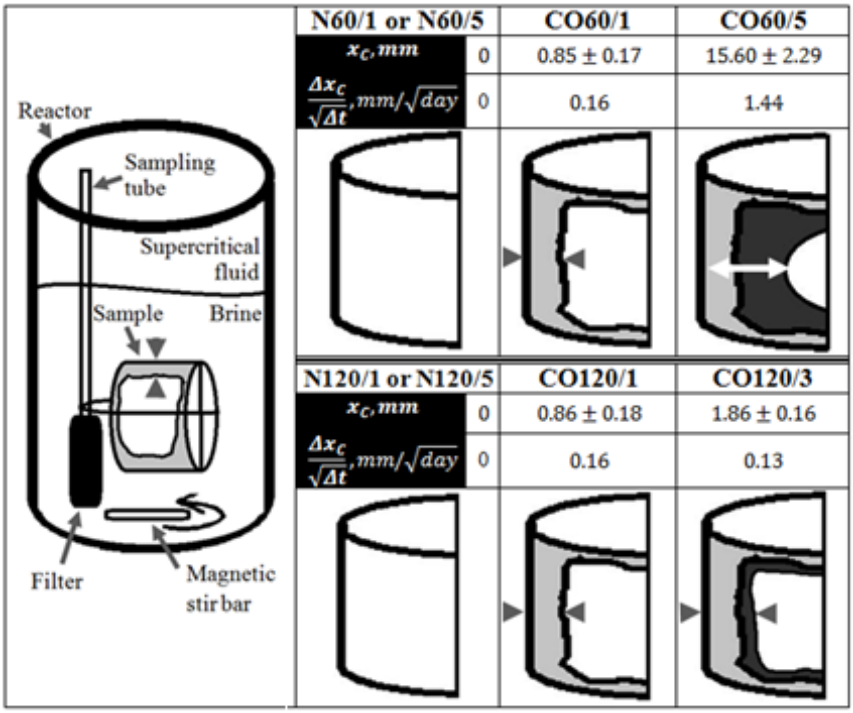

Figure 10 Synopsis of the carbonation depths for each sample and rates of change of the depths based on the linear evolution of the depths in time and the square root law of time; the calculation of the carbonation depth relatively to each sample immersed into the reactors is also shown. The design of the reactor is a schematic representation only simplified from [14]

*Table 1 The CO_2 carbonation depths and carbonation rates at 80 bar/ 120°C and at 80 bar /60°C; *, calculated values from the fitted equation per temperature.*

Days	**Carbonation Depth (mm)**		**Carbonation rate (mm/days)**	
	60°C	120°C	60°C	120°C
0	0	0	0	0
14*	0.25	0.44	0.018	0.031
30	0.85	0.86	0.028	0.029
90	5.71*	1.86	0.063	0.021
150	15.60	2.66*	0.104	0.018

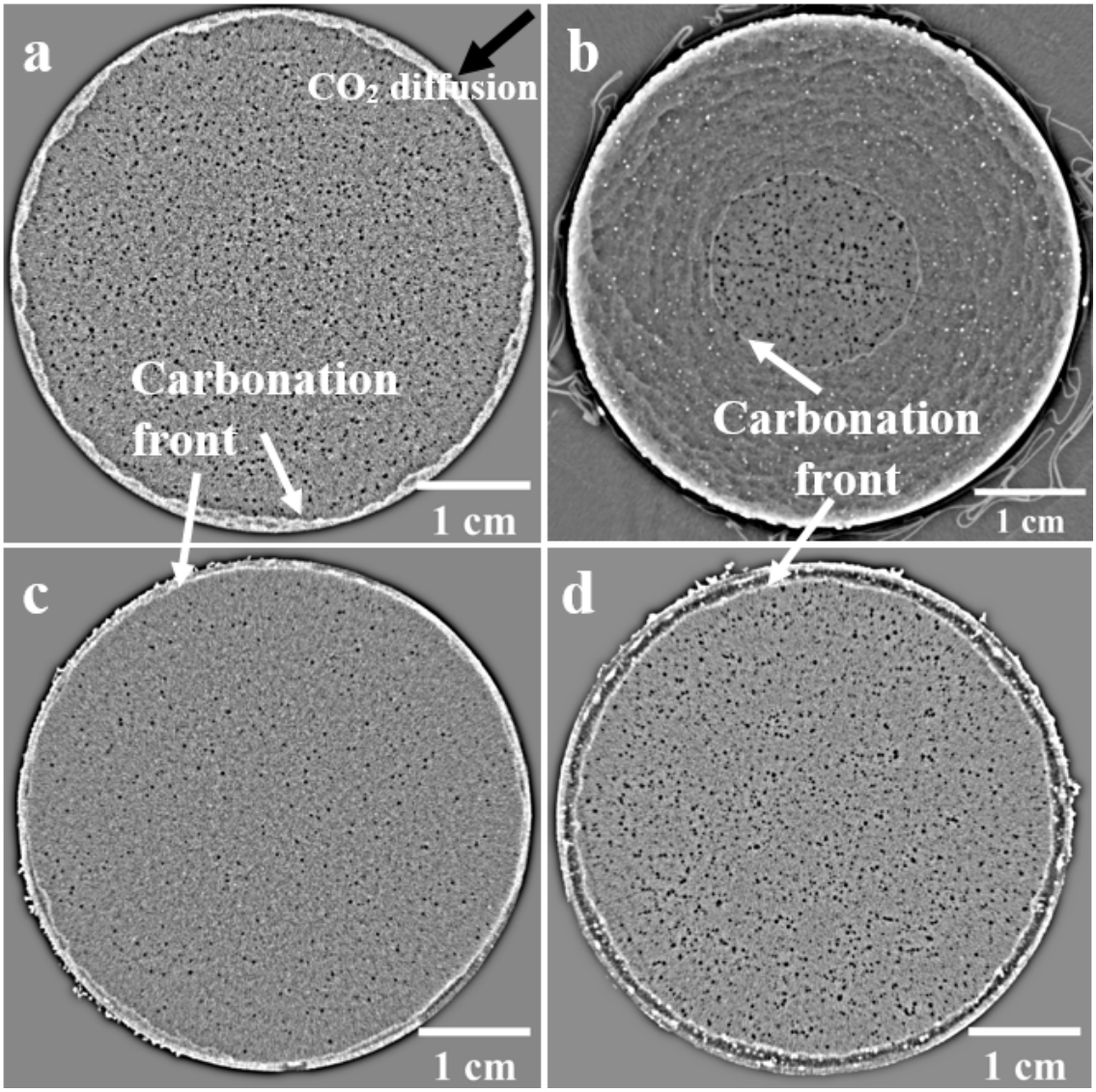

Figure 11 Visualisation of the carbonation front at the central slice of each sample at: a, 60℃ after 1 month; b, 60℃ after 5 months; c, 120℃ after 1 month; d, 120℃ after 3 months

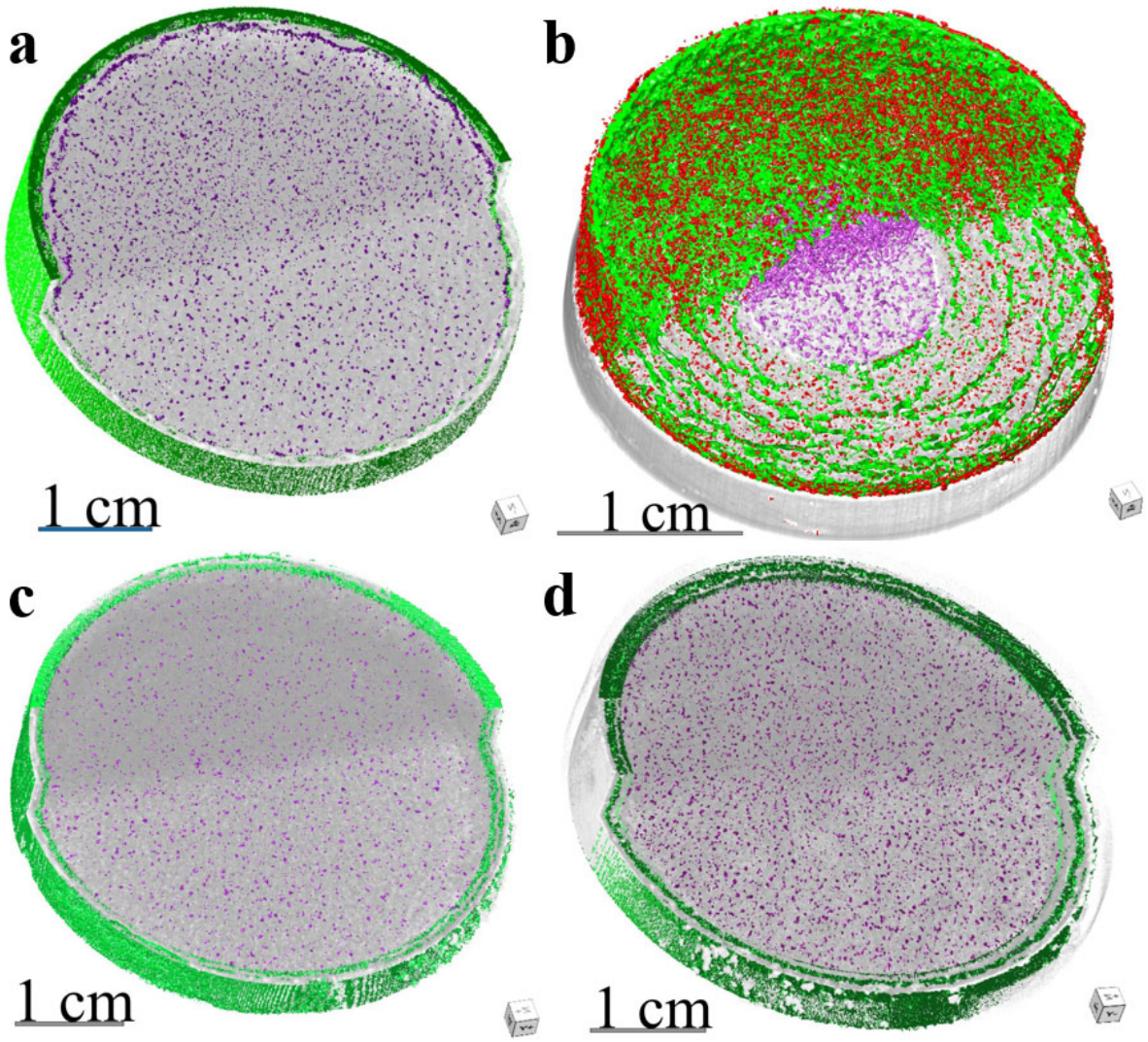

Figure 12 Orthographic projections of the carbonated samples at (a) 60℃, 1 month, (b) 60℃, 5 months, (c) 120℃, 1 month and (d) 120℃, 3 months; green, carbonation front(s); purple, voids; red, aragonite; for the visualisation, 400 slices were processed with Dragonfly 2020.1.1.809; the segmentation was done using the Otsu algorithm with threshold calculated for the each stack.

4. Summary and Conclusions

The current study presents results from the compositional characterization of class G cement under accelerated carbonation in laboratory experiments under conditions of 80 bar/ 120℃ and at 80 bar /60℃. The results of microstructural analyses provided evidence for: (1) phase alterations of a realistic cementitious grout before and after carbonation, (2) microstructure (shape, size) of the carbonation front, (3) Ca source and transport from the cement phases towards the carbonation front, (4) preferential formation of calcium carbonate

polymorphs depending upon temperature, time and degree of supersaturation (though we do not quantify it) and (5) the rate of carbonation reactions.

Our study, provided new insights in geological storage experiments, about the importance of coupling the kinetics of the 'main carbonation front', with the morphology of the front and the cement phase alterations. The results of our study bridged the gap between the mathematical description of the carbonation front [41], modelling of the time evolution of the carbonates precipitation [42] [43] and the chemical degradation of cement [10] [44] [45].

Carbonation took place within a zone of reaction, within which was a visually well-defined carbonation front at 120℃, and the presence of calcite. This indicates fast reaction rates and diffusion limited carbonation. On the contrary, the less well defined carbonation front at 60℃ along with the presence of aragonite suggests fast diffusion; the carbonation reactions were governed by the speed of saturation that were controlled by the speed of diffusion. The reactions at 60℃ were rather slow, due to the inability of aragonite (located inside air voids, see Figure 8) to transform to calcite and were governed by the supersaturation conditions. These observations were in line with the fitting of the carbonation depth evolution at 120℃ (according to the square root-law equation) and the increasing rate at 60℃ (from the lack of application of the square root-law equation). Whilst we recognise the limitations of extrapolating data from just three samples (including no carbonation -$x_c = 0cm$- at the start of the experiments), the results are nevertheless useful for comparing the carbonation rate with the power-law equation for diffusion. Basic conditions of the power-law equation (Fickian diffusion) are the diffusion through an homogeneous medium [46] and that the microstructure remains unaltered [47]. For the problem of cement carbonation, experimental studies on the mathematical equation between the carbonation depth and the elapsed time have focused on the identification of the $\boldsymbol{\alpha}$ value of the power law of time with the commonest value not to exceed 0.5 [48]. Theoretical models have also identified that the simplest case of the power

law for the problem of cement carbonation is α =0.5 [49]. However, most models were built for carbonation under atmospheric conditions and not under the studied accelerated carbonation conditions in elevated T & P conditions. It may be that some of these also had 'drying-induced shrinkage/carbonation' if the atmosphere was not water-saturated. In our study the decreasing carbonation rate at 120℃ appeared to follow the square root-law of the elapsed time showing a diffusion limited regime. On the other hand, the increasing carbonation rate at 60℃ showed deviations from the diffusion limited regime with the carbonation to be controlled by the speed of calcium carbonate precipitation.

The lack of carbonation in the central parts of the class G cement sample immersed in carbonated brine at 120℃ in our study, shows that the carbonation front has (over the timescales of our study) delayed the inner region of the cement samples from further diffusion and reaction at the tested experimental timescales. As seen the inner region at 120℃ has undergone significant alterations after just one month of reaction, in contrast to the 60℃ sample immersed into the carbonated brine. However the kinetics of carbonation at 120℃ created a carbonation zone able to seal the inner region from carbonation (see sample CO120/3) in contrast to the case of 60℃ (see sample CO60/5). That shows that phase characterisation, cannot be the sole tool for characterisation of the speed of carbonation from a carbonated cement, but needs to be coupled with kinetic analyses in order to understand better the microstructure and evolution of the carbonation zone. The morphology of the carbonation front, like its width and its chemistry, has been identified as key point for understanding the coupled diffusion/ reactive transport during accelerated cement carbonation tests at 20℃ at a CO_2 concentration 20% [50]. In fact the width of a reaction zone during reactive transport in porous media has been found to hide important evidence for the identification of the critical to carbonation step(s), i.e. diffusion and/or reaction [50]. In natural systems where the dissolution and precipitation compete with each other, the reaction zone width was found to depend on the

reaction rate and the transport regime (convection and/ or diffusion) [51] . In other words, the carbonation front was found to be a zone of transition between the dissociated old fronts and the new fronts that started to form towards the unreacted region [52].

In the case of the carbonated region at 60℃, the ill-defined front can be correlated well with the overall rate of carbonation as measured by XRCT and the presence of aragonite as evidenced from SEM and XRD. In contrast to 120℃, at 60℃ the main carbonation front was compositionally similar to the old carbonation fronts. Similar old fronts were found as relics from the dissolution of each new front and their re-precipitation towards the un-carbonated regions [53]. Fronts similar in shape with those relics or the newest carbonation front at 60℃, have been found to be formed in diffusion-controlled or reaction-controlled processes through porous materials characterised with mineralogical heterogeneities [54]. The presence of aragonite is evidence of fast supersaturation conditions [55] caused by fast diffusion through the carbonated region. In other words, the carbonation at 60℃ seemed to be characterised by a faster rate of advance of the precipitation of a new front in contrast to the dissolution fronts. It must be highlighted the 'initial' dissolution of $Ca(OH)_2$ and CSH, and also the dissolution of $CaCO_3$ behind the main reaction -precipitation- front are the main characteristics of the dissolution fronts. If the dissolution front would have moved simultaneously with the precipitation front, then at the carbonated region there would be no sign of a relic front, but a rather homogeneous silicate structure embedded with carbonate crystals.

Under downhole conditions, aragonite (which is more favourably formed at high pressures) has been claimed to transform into calcite after a few thousand years [56] [57]. Calcite is anticipated as the final product of aragonite from controlled mineral transformation due to the gradual lowering of CO_2 concentrations due to its slow mineralization within the reservoir rocks [58]. Whether the mixing of injected CO_2 with reservoir water will occur near the cement seal or not will depend on the 3D subsurface arrangement of borehole, seal, and

489 closure hosting the injected CO_2. The closer a cement is to the CO_2 injection site, the greater
490 the alteration will be [59]. However, the alterations even in long distances of the cement from
491 the injection site will occur at an extent analogous to the distance [59]; our study consisted of
492 the worst case scenario where the cement is in direct contact with the injection case at the
493 bottom of the well. For example, for a simple vertical well, mixing would be valid close to the
494 well, but for other wells which are deviated and where the injected CO_2-plume migrates away
495 from the well (*e.g.* Sleipner), the interactions of CO_2 bubbles were found (experimentally) to
496 create calcite, rendering the grout more resistant to further chemical degradation [60] [61]. It
497 must be mentioned that calcite may form, but that can still dissolve if there is sufficient CO_2
498 and undersaturated fluid leading to continuous cement degradation. For rocks that have enough
499 calcite in them to saturate the porewater in the presence of CO_2 [62] [63], then calcite in the
500 cement will clearly not dissolve, allowing for a better probability of borehole seal longevity.

501

502 **References**

503 [1] Metz B, Davidson O, De Coninck HC, Loos M, (eds.) LAM. IPCC, 2005: IPCC
504 Special Report on Carbon Dioxide Capture and Storage. Prepared by Working Group
505 III of the Intergovernmental Panel on Climate Change. 2005.

506 [2] P. Verdon J. Microseismic Monitoring and Geomechanical Modelling of CO2 Storage
507 in Subsurface Reservoirs. 2012. doi:10.1007/978-3-642-25388-1.

508 [3] Emberley S, Hutcheon I, Shevalier M, Durocher K, Mayer B, Gunter WD, et al.
509 Monitoring of fluid–rock interaction and CO2 storage through produced fluid sampling
510 at the Weyburn CO2-injection enhanced oil recovery site, Saskatchewan, Canada.
511 Appl Geochemistry 2005;20:1131–57.
512 doi:https://doi.org/10.1016/j.apgeochem.2005.02.007.

[4] White DJ. Geophysical monitoring of the Weyburn CO2 flood: Results during 10 years of injection. Energy Procedia 2011;4:3628–35. doi:https://doi.org/10.1016/j.egypro.2011.02.293.

[5] Gozalpour F, Ren SR, Tohidi B. CO2 Eor and Storage in Oil Reservoir. Oil Gas Sci Technol - Rev IFP 2005;60:537–46.

[6] Boait FC, White NJ, Bickle MJ, Chadwick RA, Neufeld JA, Huppert HE. Spatial and temporal evolution of injected CO2 at the Sleipner Field, North Sea. J Geophys Res Solid Earth 2012;117. doi:10.1029/2011JB008603.

[7] EPA. Geologic Sequestration of Carbon Dioxide Underground Injection Control (UIC) Program: Class VI Well Testing and Monitoring Guidance. 2013.

[8] Wollenweber J, Alles S, Busch A, Krooss BM, Stanjek H, Littke R. Experimental investigation of the CO2 sealing efficiency of caprocks. Int J Greenh Gas Control 2010;4:231–41. doi:https://doi.org/10.1016/j.ijggc.2010.01.003.

[9] Zakkour P, Haines M. Permitting issues for CO2 capture, transport and geological storage: A review of Europe, USA, Canada and Australia. Int J Greenh Gas Control 2007;1:94–100. doi:https://doi.org/10.1016/S1750-5836(06)00008-9.

[10] Kutchko BG, Strazisar BR, Dzombak DA, Lowry G V, Thaulow N. Degradation of Well Cement by CO2 under Geologic Sequestration Conditions. Environ Sci Technol 2007;41:4787–92. doi:10.1021/es062828c.

[11] Zivica V, Bajza A. Acidic attack of cement based materials — a review.: Part 1. Principle of acidic attack. Constr Build Mater 2001;15:331–40. doi:https://doi.org/10.1016/S0950-0618(01)00012-5.

[12] Matteo EN, Scherer GW. Experimental study of the diffusion-controlled acid

536 degradation of Class H Portland cement. Int J Greenh Gas Control 2012;7:181–91.
537 doi:https://doi.org/10.1016/j.ijggc.2011.07.012.

538 [13] Duguid A, Scherer GW. Degradation of oilwell cement due to exposure to carbonated
539 brine. Int J Greenh Gas Control 2010;4:546–60.

540 [14] Rochelle CA, Milodowski AE. Carbonation of borehole seals: Comparing evidence
541 from short-term laboratory experiments and long-term natural analogues. Appl
542 Geochemistry 2013;30:161–77. doi:https://doi.org/10.1016/j.apgeochem.2012.09.007.

543 [15] Opedal N, Lavrov A, Todorovic J, Torsæter M. The importance of shale caprock
544 damage for well integrity. Int J Greenh Gas Control 2018;74:182–90.
545 doi:10.1016/J.IJGGC.2018.04.007.

546 [16] William Carey J, Svec R, Grigg R, Zhang J, Crow W. Experimental investigation of
547 wellbore integrity and CO2–brine flow along the casing–cement microannulus. Int J
548 Greenh Gas Control 2010;4:272–82. doi:10.1016/J.IJGGC.2009.09.018.

549 [17] Walsh SDC, Mason HE, Du Frane WL, Carroll SA. Experimental calibration of a
550 numerical model describing the alteration of cement/caprock interfaces by carbonated
551 brine. Int J Greenh Gas Control 2014;22:176–88.
552 doi:https://doi.org/10.1016/j.ijggc.2014.01.004.

553 [18] Luquot L, Abdoulghafour H, Gouze P. Hydro-dynamically controlled alteration of
554 fractured Portland cements flowed by CO2-rich brine. Int J Greenh Gas Control
555 2013;16:167–79. doi:10.1016/J.IJGGC.2013.04.002.

556 [19] Carey JW, Wigand M, Chipera SJ, WoldeGabriel G, Pawar R, Lichtner PC, et al.
557 Analysis and performance of oil well cement with 30 years of CO2 exposure from the
558 SACROC Unit, West Texas, USA. Int J Greenh Gas Control 2007;1:75–85.

559 doi:https://doi.org/10.1016/S1750-5836(06)00004-1.

560 [20] Gawel K, Todorovic J, Liebscher A, Wiese B, Opedal N. Study of Materials Retrieved
561 from a Ketzin CO2 Monitoring Well. Energy Procedia 2017;114:5799–815.
562 doi:https://doi.org/10.1016/j.egypro.2017.03.1718.

563 [21] Scherer GW, Kutchko B, Thaulow N, Duguid A, Mook B. Characterization of cement
564 from a well at Teapot Dome Oil Field: Implications for geological sequestration. Int J
565 Greenh Gas Control 2011;5:115–24. doi:https://doi.org/10.1016/j.ijggc.2010.06.010.

566 [22] Fabbri A, Corvisier J, Schubnel A, Brunet F, Goffé B, Rimmele G, et al. Effect of
567 carbonation on the hydro-mechanical properties of Portland cements. Cem Concr Res
568 2009;39:1156–63. doi:https://doi.org/10.1016/j.cemconres.2009.07.028.

569 [23] Thiery M, Villain G, Dangla P, Platret G. Investigation of the carbonation front shape
570 on cementitious materials: Effects of the chemical kinetics. Cem Concr Res
571 2007;37:1047–58. doi:10.1016/J.CEMCONRES.2007.04.002.

572 [24] Morse JW, Arvidson RS, Lüttge A. Calcium Carbonate Formation and Dissolution.
573 Chem Rev 2007;107:342–81. doi:10.1021/cr050358j.

574 [25] Miao X, Zhang L, Wang Y, Wang L, Fu X, Gan M, et al. Characterisation of wellbore
575 cement microstructure alteration under geologic carbon storage using X-ray computed
576 micro-tomography: A framework for fast CT image registration and carbonate shell
577 morphology quantification. Cem Concr Compos 2020;108:103524.
578 doi:https://doi.org/10.1016/j.cemconcomp.2020.103524.

579 [26] Anna P de, Jimenez-Martinez J, Tabuteau H, Turuban R, Le Borgne T, Derrien M, et
580 al. Mixing and Reaction Kinetics in Porous Media: An Experimental Pore Scale
581 Quantification. Environ Sci Technol 2014;48:508–16. doi:10.1021/es403105b.

582 [27] Myers R. An Investigation of ASTM Type I Cement for Oilwell Application in the
583 Appalachian and Michigan Basins. SPE East Reg Conf Proc 2000. doi:10.2118/65621-
584 MS.

585 [28] Chen B, Harp DR, Lu Z, Pawar RJ. Reducing uncertainty in geologic CO2
586 sequestration risk assessment by assimilating monitoring data. Int J Greenh Gas
587 Control 2020;94:102926. doi:10.1016/J.IJGGC.2019.102926.

588 [29] Walter J. Safety management at the frontier: Cooperation with contractors in oil and
589 gas companies. Saf Sci 2017;91:394–404. doi:10.1016/J.SSCI.2016.09.001.

590 [30] Li Z, Fang F, Tang X, Cai N. Effect of Temperature on the Carbonation Reaction of
591 CaO with CO2. Energy & Fuels 2012;26:2473–82. doi:10.1021/ef201543n.

592 [31] Liu S, Guan X, Zhang H, Wang Y, Gou M. Revealing the Microstructure Evolution
593 and Carbonation Hardening Mechanism of β-C2S Pastes by Backscattered Electron
594 Images. Materials (Basel) 2019;12. doi:10.3390/ma12091561.

595 [32] Liu W, Li Y-Q, Tang L-P, Dong Z-J. XRD and 29Si MAS NMR study on carbonated
596 cement paste under accelerated carbonation using different concentration of CO2.
597 Mater Today Commun 2019;19:464–70. doi:10.1016/J.MTCOMM.2019.05.007.

598 [33] Jiande H, Wei S, Ganghua P, Wang C. Monitoring the Evolution of Accelerated
599 Carbonation of Hardened Cement Pastes by X-Ray Computed Tomography. J Mater
600 Civ Eng 2013;25:347–54. doi:10.1061/(ASCE)MT.1943-5533.0000610.

601 [34] Chang R, Kim S, Lee S, Choi S, Kim M, Park Y. Calcium Carbonate Precipitation for
602 CO2 Storage and Utilization: A Review of the Carbonate Crystallization and
603 Polymorphism . Front Energy Res 2017;5:17.

604 [35] Chu DH, Vinoba M, Bhagiyalakshmi M, Hyun Baek II, Nam SC, Yoon Y, et al. CO2

605 mineralization into different polymorphs of CaCO3 using an aqueous-CO2 system.
606 RSC Adv 2013;3:21722–9. doi:10.1039/C3RA44007A.

607 [36] Connolly Albuquerque, NM (USA). Dept. of Geology] JR [New MU, Nimick
608 Albuquerque, NM (USA)] FB [Sandia NL. Mineralogic and chemical data supporting
609 heat capacity determination for tuffaceous rocks. United States: 1990.
610 doi:10.2172/137663.

611 [37] Bish DL, Reynolds RC. 4. SAMPLE PREPARATION FOR X-RAY DIFFRACTION.
612 In: Bish DL, Post JE, editors., De Gruyter; 2018, p. 73–100.
613 doi:doi:10.1515/9781501509018-007.

614 [38] Baur I, Keller P, Mavrocordatos D, Wehrli B, Johnson CA. Dissolution-precipitation
615 behaviour of ettringite, monosulfate, and calcium silicate hydrate. Cem Concr Res
616 2004;34:341–8. doi:10.1016/j.cemconres.2003.08.016.

617 [39] Kocaba V. Development and evaluation of methods to follow microstructural
618 development of cementitious systems including slags. EPFL PP - Lausanne, n.d.
619 doi:10.5075/epfl-thesis-4523.

620 [40] Jennings HM. Refinements to colloid model of C-S-H in cement: CM-II. Cem Concr
621 Res 2008;38:275–89. doi:https://doi.org/10.1016/j.cemconres.2007.10.006.

622 [41] Aiki T, Muntean A. A free-boundary problem for concrete carbonation: Front
623 nucleation and rigorous justification of the pt -law of propagation. vol. 15. 2013.
624 doi:10.4171/IFB/299.

625 [42] Fabbri A, Jacquemet N, Seyedi DM. A chemo-poromechanical model of oilwell
626 cement carbonation under CO2 geological storage conditions. Cem Concr Res
627 2012;42:8–19. doi:10.1016/J.CEMCONRES.2011.07.002.

628 [43] Brunet J-PL, Li L, Karpyn ZT, Huerta NJ. Fracture opening or self-sealing: Critical
629 residence time as a unifying parameter for cement–CO2–brine interactions. Int J
630 Greenh Gas Control 2016;47:25–37. doi:https://doi.org/10.1016/j.ijggc.2016.01.024.

631 [44] Gan M, Zhang L, Miao X, Wang Y, Fu X, Bai M, et al. Micro-CT Characterization of
632 Wellbore Cement Degradation in SO_4^{2-}–Bearing Brine under Geological CO_2 Storage
633 Environment. Geofluids 2019;2019:5164010. doi:10.1155/2019/5164010.

634 [45] Li Q, Lim YM, Flores KM, Kranjc K, Jun Y-S. Chemical Reactions of Portland
635 Cement with Aqueous CO2 and Their Impacts on Cement's Mechanical Properties
636 under Geologic CO2 Sequestration Conditions. Environ Sci Technol 2015;49:6335–
637 43. doi:10.1021/es5063488.

638 [46] Glasser F. Application of inorganic cements to the conditioning and immobilisation of
639 radioactive wastes. Handb Adv Radioact Waste Cond Technol 2011:67–135.
640 doi:10.1533/9780857090959.1.67.

641 [47] Woyciechowski P, Woliński P, Adamczewski G. Prediction of Carbonation Progress
642 in Concrete Containing Calcareous Fly Ash Co-Binder. Mater (Basel, Switzerland)
643 2019;12:2665. doi:10.3390/ma12172665.

644 [48] du béton F. Structural Concrete Textbook - Vol 3, first edition: Textbook on
645 Behaviour, Design and Performance: Updated knowledge of the CEB/FIP Model Code
646 1990 - Volume 3. International Federation for Structural Concrete; 1999.

647 [49] Papadakis VG, Vayenas CG, Fardis MN. A reaction engineering approach to the
648 problem of concrete carbonation. AIChE J 1989;35:1639–50.
649 doi:10.1002/aic.690351008.

650 [50] Wan K, Xu Q, Wang Y, Pan G. 3D spatial distribution of the calcium carbonate caused

651 by carbonation of cement paste. Cem Concr Compos 2014;45:255–63.

652 [51] Kondratiuk P, Tredak H, Upadhyay V, Ladd AJC, Szymczak P. Instabilities and finger
653 formation in replacement fronts driven by an oversaturated solution. J Geophys Res
654 Solid Earth 2017;122:5972–91. doi:10.1002/2017JB014169.

655 [52] Iyer J, Walsh SDC, Hao Y, Carroll SA. Incorporating reaction-rate dependence in
656 reaction-front models of wellbore-cement/carbonated-brine systems. Int J Greenh Gas
657 Control 2017;59:160–71. doi:10.1016/J.IJGGC.2017.01.019.

658 [53] Rimmelé G, Barlet-Gouédard V, Porcherie O, Goffé B, Brunet F. Heterogeneous
659 porosity distribution in Portland cement exposed to CO2-rich fluids. Cem Concr Res
660 2008;38:1038–48.

661 [54] Min T, Gao Y, Chen L, Kang Q, Tao W. Changes in porosity, permeability and surface
662 area during rock dissolution: Effects of mineralogical heterogeneity. Int J Heat Mass
663 Transf 2016;103:900–13. doi:10.1016/J.IJHEATMASSTRANSFER.2016.07.043.

664 [55] Hu Z, Deng Y. Supersaturation Control in Aragonite Synthesis Using Sparingly
665 Soluble Calcium Sulfate as Reactants. J Colloid Interface Sci 2003;266:359–65.
666 doi:10.1016/S0021-9797(03)00699-4.

667 [56] BUDD DA. Aragonite-to-calcite transformation during fresh-water diagenesis of
668 carbonates: Insights from pore-water chemistry. GSA Bull 1988;100:1260–70.
669 doi:10.1130/0016-7606(1988)100<1260:ATCTDF>2.3.CO;2.

670 [57] Duguid A. An estimate of the time to degrade the cement sheath in a well exposed to
671 carbonated brine. Energy Procedia 2009;1:3181–8.
672 doi:https://doi.org/10.1016/j.egypro.2009.02.101.

673 [58] Carroll SA, McNab WW, Torres SC. Experimental Study of Cement - Sandstone/Shale

674 - Brine - CO2 Interactions. Geochem Trans 2011;12:9. doi:10.1186/1467-4866-12-9.

675 [59] Zhang M, Bachu S. Review of integrity of existing wells in relation to CO2 geological
676 storage: What do we know? Int J Greenh Gas Control 2011;5:826–40.
677 doi:10.1016/J.IJGGC.2010.11.006.

678 [60] Hidalgo A, Domingo C, Garcia C, Petit S, Andrade C, Alonso C. Microstructural
679 changes induced in Portland cement-based materials due to natural and supercritical
680 carbonation. J Mater Sci 2008;43:3101–11. doi:10.1007/s10853-008-2521-5.

681 [61] García-González CA, el Grouh N, Hidalgo A, Fraile J, López-Periago AM, Andrade C,
682 et al. New insights on the use of supercritical carbon dioxide for the accelerated
683 carbonation of cement pastes. J Supercrit Fluids 2008;43:500–9.
684 doi:10.1016/J.SUPFLU.2007.07.018.

685 [62] Kim K, Vilarrasa V, Makhnenko R. CO2 Injection Effect on Geomechanical and Flow
686 Properties of Calcite-Rich Reservoirs. Fluids 2018;3:66. doi:10.3390/fluids3030066.

687 [63] Xiao T, McPherson B, Bordelon A, Viswanathan H, Dai Z, Tian H, et al.
688 Quantification of CO2-cement-rock interactions at the well-caprock-reservoir interface
689 and implications for geological CO2 storage. Int J Greenh Gas Control 2017;63:126–
690 40. doi:https://doi.org/10.1016/j.ijggc.2017.05.009.

691